Check for updates

Atmospheric plasma treatments of cashmere: The role of nanoscale sizing in the spray coating processing

R. Barni[1], H. E. Roman[1], A. Citterio[2], G. Leonardi[2] and C. Riccardi[1]*

[1]Dipartimento di Fisica G. Occhialini, Universitá degli Studi di Milano - Bicocca, Milan, Italy,
[2]Dipartimento di Chimica, Materiali ed Ingegneria Chimica "G.Natta", Politecnico di Milano, Milan, Italy

We discuss the effects of air atmospheric plasma interaction with the surface of a textile. We studied how plasma can promote changes in its texture and roughness at nano- and micro-meter scales, having an impact on the improvement of such macroscopic properties as hydro/oleo-repellency and pilling, without altering the hand assessment quality of the textile. These results are obtained by analyzing images taken using electron microscopy. We studied both the fluctuations of the image intensity at the fiber surfaces and their Fourier transforms at the sub-micrometer scales. As a case study, we have analyzed the modifications of a cashmere fabric and the improvement of finishing using resin spray coating. We observe a better efficiency when resin is applied to a plasma-treated sample. This result has been traced to the modifications that plasma induces on the surface at the nanoscale. This opens up wide perspectives to the use of plasma technology for the whole textile industrial sector.

KEYWORDS

atmospheric pressure plasma, plasma processing, nanostructures, cashmere, spray coating, textile finishing

Introduction

Nanotechnology contributes to the opportunity in developing improved materials with advanced properties for their utilization in different application fields. Nanostructured materials, nanoparticles embedded in material matrices, and metamaterials are of great interest in applications from energy (Trifiletti et al., 2013; Liu et al., 2020), the environment, and catalysis (Wang et al., 2018) to the manufacturing (Dell'Orto et al., 2017) and the textile sectors (Zhao et al., 2018).

Several natural and synthetic polymer substrates and fibers have been the subject of studies aimed at improving surface performances and different functionalities (Heinzel and Stewart, 2021) through nanoscale processing, like, for instance, nano-coatings (Dell'Orto et al., 2014), nano-structuring (Saleem and Zaidi, 2020), as well as the

incorporation of nanoparticles (Radetić and Marković, 2019). Different nanotechnologies are employed, some of which are sol–gel (Abramova et al., 2020), plasma etching (Porto et al., 2019), plasma deposition (Zanini et al., 2018b), grafting of specific chemical groups (Zanini et al., 2016b), and several wet treatments (Venkatraman et al., 2021).

Nano-finishing applies colloidal solution or ultrafine dispersion of nanomaterials to a textile material enhancing some of the functionalities. The sol–gel technique has been largely used in textiles for antibacterial properties and medical applications, for instance, employing nanosized silver colloidal solutions (Abramova et al., 2020) and zinc oxides nanoparticles for the surface activation of polymeric natural fibers (Noman et al., 2021). In nano-coating, a thin film whose thickness is less than 1 μm is deposited on the substrate in order to impart advanced functionality (hydro-repellency, oleo-repellency, flame retardant, etc.) (Peng et al., 2019). In this context, wool fibers, including alpaca wool (Memon et al., 2018a,b; Khoso et al., 2016) and cashmere (Zanini et al., 2015), have been explored and their properties studied in order to improve finishing and dyeing processing. Different processes have been analyzed for dyeing and finishing purposes, such as UV curing (Wang et al., 2020), nano-silver particle inclusion for antibacterial properties (Memon et al., 2018a), low vacuum plasma (Haji et al., 2020), and atmospheric plasma (Zanini et al., 2015).

The application of nonthermal atmospheric pressure plasmas and nanotechnology in the fields of textiles is very promising to promote and/or impart new functionalities because most of the processing is dry and this makes its use in the industry very challenging (Singh et al., 2020). Many studies deal with plasma treatments of wool at low plasma pressure, where the wool surface undergoes both oxidation and an increase of roughness (Peran et al., 2020; Haji, 2020a,b). In the latter, low-pressure plasma treatments are reported for hydrophilicity, antimicrobial properties, and for increasing the dyeing affinity. From an industrial point of view low-pressure plasma treatments need long processing times and expensive equipment. Atmospheric pressure plasma treatments of wool have been performed to increase the dyeing capacity, to improve the mechanical properties and as pretreatment to enhance the coating properties (Zanini et al., 2015; Bulut and Sana, 2018; Najar et al., 2018), and they appear most promising for the industrial sector as they adapt well to the associated fabrication requirements.

A largely important open issue for the textile industry is related to the adhesion of natural and synthetic fibers to coating and resins to impart different functionalities. Here the research is aimed to decrease the use of chemicals and water in industrial finishing processing (Radetić and Marković, 2019). In most of the existing literature, wool characteristics are studied by analyzing in detail their chemical modifications by FT-IR, XPS, EDX, and by performing morphological investigations by means of AFM and SEM at the microscopic scale. However, a detailed study of the morphological alterations of wool after atmospheric plasma treatments, and its role in the surface pretreatment, has not been conducted yet. Moreover, it is not even clear whether an improvement in texture roughness can improve the expected wool properties.

In a recent study, atmospheric plasma has been used for increasing the adhesion to coatings on wool and cashmere textiles (Zanini et al., 2016a), where plasma is used as pretreatment, showing that plasma increases the chemical affinity of fibers to resins used to realize hydro- and oleo-repellent surfaces. Furthermore, it has also been shown that plasma acts at the microscopic scale favoring a better resin adhesion to the fibers (Zanini et al., 2016a). This leads to better efficiency of the hydro-oleo effect and also helps save resin in the coating process. In addition, the role of surface morphology in the problem remains to be understood.

Recently, it has been shown that surface tension does not only depend on chemistry, but also on the nano-structuring and micro-structuring of the surface. The models by Cassie and Baxter (Murakami et al., 2014; Nagayama and Zhang, 2020) show that the macroscopic response of a liquid in the form of a drop on a surface is modified by the geometric structure of the surface at the microscopic level, not just by surface chemistry. We cannot therefore ignore the morphological effect.

This study deals with the role of plasma pretreatment at the nanoscale, in the nano-structuring of fibers, and to the effects of fiber nano-structuring on the macroscopic textile functionalities. In particular, the presence of different nano- and micro-length scales, emerging during the plasma processing, has been investigated to better understand the plasma–surface interaction mechanisms and to optimize and control resin adhesion on the fiber surfaces. An improved understanding of this topic provides a way for developing progressive sustainable textiles in the upcoming years with the probability of improving the life quality. Based on our previous studies on the plasma-induced chemical and morphological characteristics on different material surfaces, this study deals with specific research on the different scale lengths involved in the plasma pretreatments and their role in the coating performances. In this study, we consider pure cashmere as the test textile.

In this study, we consider pure cashmere as our textile target. To this end, we deal with the investigation of the effects of plasma treatment on fiber morphology and texturing on the different fiber spatial scales, as well as on the correlation between the textile nano-texture and the enhancement of the spray coating properties. We find that an enhancement of the coating properties, such as water/oleo-repellency and pilling, is caused by plasma-induced sub-micrometric sizing during the pretreatment which facilitates the covering of the resin on the fibers, maintaining the hand assessment quality of the textile.

Materials and methods

Our aim is to study the effect of the plasma exposition on the morphology and the nano-texturing of cashmere surfaces. This, in turn, affects a variety of properties of the material, both its finishing appearance (see for instance the touch or hardness, softness or pilling resistance) and its capability to interact with different agents (think, for instance, adhesion changes for resin finishing or wettability and dyeability). For our purpose, we selected a highly valued textile material, in our case a commercial pure cashmere fabric, supplied by LoroPiana (Quarona, Italy), a renowned company specializing in luxury textiles. Cashmere is a complex biological fiber made of proteins that provide flexibility and excellent performance qualities. In particular, the fibers are composed of overlapping cuticles, a feature that we will discuss in our analysis (Leeder, 1984; Rouette, 1995). Single fibers have diameters of about (8–12) μm. A regular warp and weft thread mesh (PPI = 100, EPI = 100, 45/2 Nm) composes the fabric, with a grammage of 200 g/m^2 and a thickness of about 0.3 mm. Such textile was selected because it is composed of homogeneous fibers of pure cashmere, and it is already finished, combed, razed, and dyed (in black).

Plasma treatments have been performed with a planar Dielectric Barrier Discharge (DBD) reactor (Kogelschatz, 2003). This is an easily scalable system to treat fabrics since it is operated at atmospheric pressure and it could be applied also to wide pieces (like those produced by industrial weaving) and inserted in lines or in a roll-to-roll environment. The treatments discussed here were performed on a laboratory device (S2V-2, by Tigres GmbH) on A4 size fabrics (Dell'Orto et al., 2014). The fabric samples were placed directly on the upper side of the dielectric surface (here PTFE, 1 mm thick) shielding the stainless-steel plane ground electrode (see **Figure 1**). A moving electrode head slid back and forth above the dielectric surface. Its velocity varied between 0.7 m/min and 7 m/min. The electrodes, a couple of parallel alumina-insulated copper cylinders (L = 220 mm length, 8–12 mm diameter, 20 mm separation), were passed at a fixed distance from the dielectric surface (here 2 mm). They were fed, through a high-voltage transformer, by a power generator (maximum power, W = 450 W), which also monitored the power adsorption and the working frequency. Both electrodes are driven, during their motion, by a sinusoidal voltage signal, whose actual amplitude and frequency vary in order for the electrical discharge to match the pre-fixed power adsorption level (Zanini et al., 2016a). More details on the electrical discharge properties are discussed in the following and additional details can be found in Piferi et al. (2021) and Biganzoli et al. (2013b,a). A gas–vapor mixing station, based on mass flowmeters and an evaporator (EL-Flow and CEM by Bronkhorst), was used to prepare a suitable gas mixture which is flown through the head between the HV electrodes with an injection flute. The gas mixture spread into the gap, where it is ignited by the electrical discharge, and it is dispersed away mixing with the ambient air. Gas mixtures used included air dry and wet, with the addition of water vapor and nitrogen (Zanini et al., 2018a, 2015).

In addition to the direct effect of exposition to plasma, we also focused on the finishing of the textiles. The use of suitable resins could achieve modifications in performances such as hydro-repellency, oleo-repellency, or, very important in the case of wool, pilling. Our aim is to discuss the improvement that plasma treatment could achieve by promoting the use of more efficient methods of resin application, in this case spraying compared to impregnation, rather than using plasma directly for finishing. Spraying allows a substance to be applied quickly onto a material surface in a uniform fashion, using only a limited amount of solvents and allowing delivery of a carefully controlled dose of the substance. It has obvious advantages with respect to a traditional bath, but it is usually less efficient and requires low viscosity of the dispersion employed. We wondered whether plasma treatment of the surfaces in advance could help the spraying process. Untreated and plasma-treated fabrics were exposed to a pneumatic sprayer being able to process solutions whose viscosity does not exceed 100 cP. Here, we discuss the use of two kinds of commercial polyurethane resins, a cationic one from aliphatic isocyanate, with silicon in the chain, and another similar one but containing fluorocarbon groups. (CNS and FCR Lamgard 48 both from Lamberti Chemicals). Both resins were dispersed into surfactant-free solvents, here simply water, with a typical dry residual of 1% and in a case 2%. Dispersion sizes ranged between 100 and 2,000 nm, and the active component was about 32% of the resin weight. After the spraying, heating at 130° for 4 min was applied to help resin fixing and drying of the fabrics.

A key instrument that we employed to investigate the plasma modification of the textiles was the scanning electron microscope (SEM). This analysis allows us to record with a high resolution the structure of the outermost surface of a material, down to the nanometer scale. EVA-50-EP, by Zeiss, was used with an electron beam energy of 10 kV. In addition, the composition of the material at the surface could be measured by an energy-dispersive X-ray system (EDX), an Oxford Inca Energy 200, by Inca. Different magnifications of the surface were recorded into digitized images for subsequent analysis, spanning the whole range of scales suitably (**Figure 2**). EDX analysis refers to high-resolution spots about $1 \times 1 \mu$m^2 in size. Electron beam energy was reduced to less than 1 kV to reduce penetration below the surface, and no metal was deposited onto it to preserve at best the original topography of the treated and untreated samples. However, when considering a surface composition evaluated by EDX, it should be remembered that this refers to a depth of about 10 μm.

A standard assessment of the wettability of a particular substance could be embodied in the measurement of the static water contact angle (WCA) (Le et al., 1996). We employed
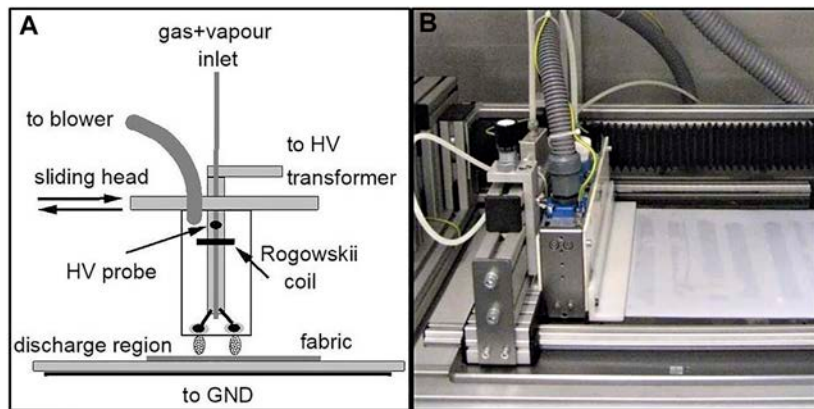
FIGURE 1
(A) DBD setup, with the moving electrode head sliding above the grounded, insulated plate and the fabric sample to be treated over there. The gas–vapor mix injection point is also shown. **(B)** The laboratory device.

FIGURE 2
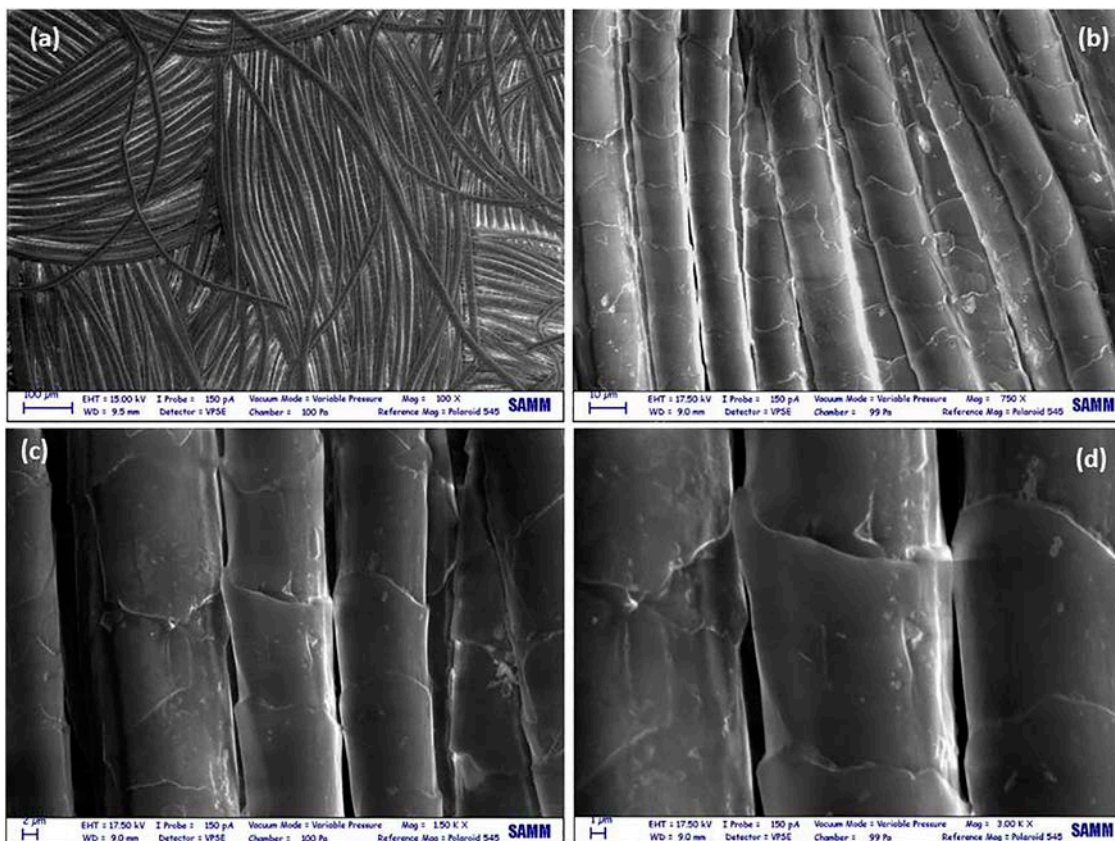A series of SEM images with four increasing magnifications: **(A)** ×100, **(B)** ×750, **(C)** ×1,500, and **(D)** ×3,000, of the untreated cashmere fabric sample. An approximate vertical orientation of the fibers was chosen at the highest scales.

DataPhysics OCA-20 instruments, where $3\,\mu L$ droplets of deionized water have been deposited on the fabric surface to be evaluated. Reported measurements and their dispersion have been calculated by averaging 10 data taken at different locations on the fabric sample. Hydro-repellence and oleo-repellence properties have been tested using standard polar and apolar kit-tests. In particular, hydro-repellence was measured by a 3-M standard test (AATCC 193–2007) based on wetting in water/isopropyl alcohol solutions, whereas oleo-repellency was tested (ISO 14419–2010) by measuring wetting by liquid hydrocarbons of different surface tension (see Zanini et al., 2016a) for more details). Higher numbers indicate a better repellency grade. The tests were repeated on different spots of the samples to be sure of the uniformity. They provide an integer grade, from which dispersion can be estimated. Another important property of a cashmere fabric is its resistance to pilling. The anti-pilling grade was evaluated using the standard ASTM-D3512, based on the random tumbling pilling method (ASTM, 2017). Again, higher grades (within the 0–5 range) indicate better anti-pilling fabrics.

SEM images from fabric samples were converted into a matrix using a numerical integer scale (0–255), corresponding to the local pixel intensity in greyscale. The matrix could be analyzed using its 2D Fourier discrete transform (DFT with Matlab software FFT2),

$$F\left(\lambda_x, \lambda_y\right) = \sum_{n_x} \sum_{n_y} I\left(n_x, n_y\right) e^{2\pi i \left(n_x/\lambda_x + n_y/\lambda_y\right)}, \qquad (1)$$

where n_x and n_y indices run over the image pixels along the horizontal and vertical axes. The spatial scales $\lambda_{x,y}$ are determined by the image size in pixels and by the magnification. In this way, the different spatial scales and their correlation in the images have been measured (Brigham, 1988; James, 2022). However, it is difficult to compare and extract quantitative data from the 2D FFT matrices. We then proceeded in two ways. A one-dimensional FFT vector signal could be calculated from the full 2D FFT by numerical integration of one of the two dimensions,

$$F(\lambda) = \sum_{n_x} \left(\sum_{n_y} I\left(n_x, n_y\right) \right) e^{2\pi i n_x/\lambda_x}. \qquad (2)$$

This is mostly meaningful when images already show fiber orientation parallel to one-dimension. In this case, the result reflects the fiber characteristics in the longitudinal as well as transversal directions. Since images were transformed in matrices, it was also possible to extract single one-dimensional sections, alternatively, rows or lines, when the fibers are suitably oriented, which was ensured during SEM imaging sessions. If necessary, digitized images were rotated for better orienteering, using commercial digital picture elaboration software. At the lowest magnification, the orientation simply approximately follows the fiber laying. At higher magnifications, fibers were aligned to the vertical axis.
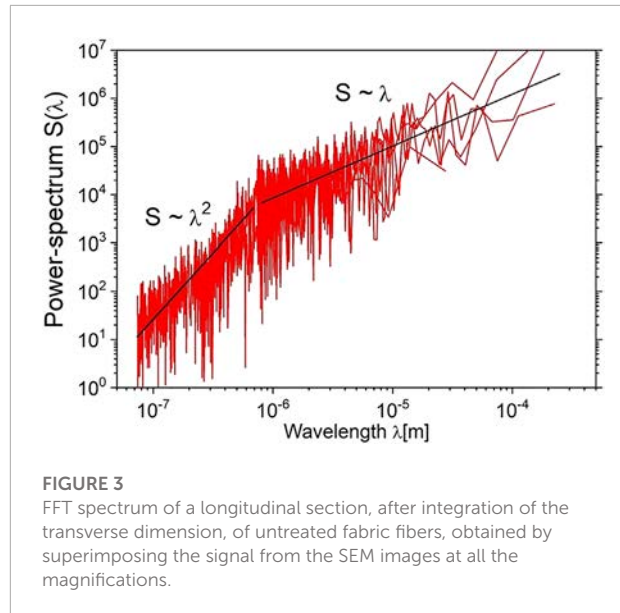

FIGURE 3
FFT spectrum of a longitudinal section, after integration of the transverse dimension, of untreated fabric fibers, obtained by superimposing the signal from the SEM images at all the magnifications.

Care was paid to include the complete transverse section of the selected fibers and to span at least one of the cuticles' superposition areas, even at the highest resolution, since these are the two main features, with their typical spatial scale which is generally present in each of the samples (see Figure 2). Then, the monodimensional FFT obtained from transverse integration was calculated from images at different magnifications (between ×100 to ×3,000) as shown in Figure 3. They have been joined in order to obtain a single function of the spatial scale from about 80 nm to 0.4 mm. The power spectrum, $S(\lambda)) = |F(\lambda)|^2$, is shown in Figure 3 on a log–log scale to underline the overall trends, which we will discuss.

Finally, we have focused on the sub-micrometric scales. To tackle the problem arising from inhomogeneities in the SEM images, we used only the parts of the images limited to a single cuticle. This excludes from the analysis the structures at the edges of the cuticles, their superposition and entanglement, and also the structure formed by the resin between adjoining fibers. A numerical scale corresponding to the greyscale (0–255) was used as intensity.

An example of such an intensity graph is shown in Figure 4 where a longitudinal, parallel to fiber, line of about $50\,\mu m$ length is analyzed. The transition across the cuticles is clearly seen as peaks. In order to investigate the roughness at the sub-micrometric level, the analysis was then restricted to the regions between the edges.

Generally, a second-order polynomial baseline, $y_{fit} = ax^2 + bx + c$, is sufficient to reproduce the average trend inside such regions. The parameters a, b, and c can be easily obtained by least square minimization. After such fit, the sub-micrometric roughness can be calculated by taking the standard
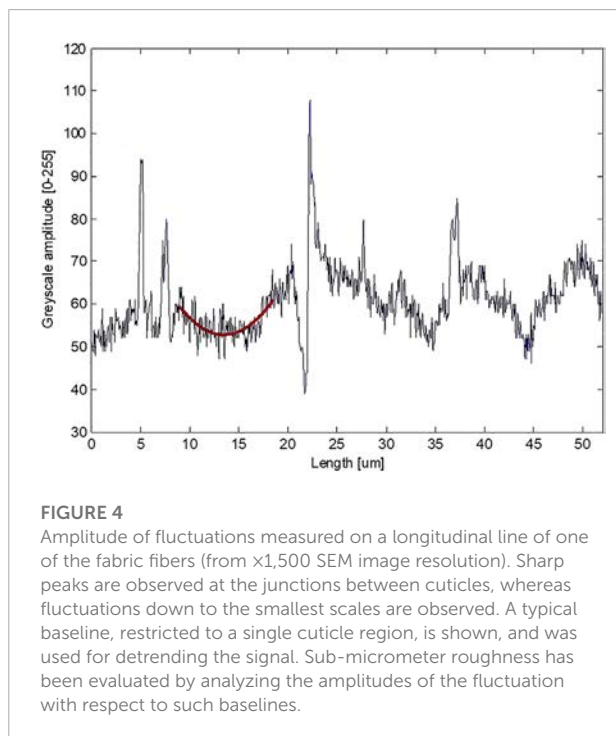
FIGURE 4
Amplitude of fluctuations measured on a longitudinal line of one of the fabric fibers (from ×1,500 SEM image resolution). Sharp peaks are observed at the junctions between cuticles, whereas fluctuations down to the smallest scales are observed. A typical baseline, restricted to a single cuticle region, is shown, and was used for detrending the signal. Sub-micrometer roughness has been evaluated by analyzing the amplitudes of the fluctuation with respect to such baselines.

deviation, R, from the baseline, according to,

$$R = \frac{1}{256} \sqrt{\frac{1}{N} \sum_{n=1}^{N} [y(x_n) - y_{\text{fit}}(x_n)]^2}. \tag{3}$$

This procedure ensures that larger scale variations do not enter the evaluation. To reduce the spread and to evaluate the precision of our estimated roughness, R, datasets of about 20 approximately longitudinal lines were selected from different areas of the images. Averaging of the individual roughness was then performed, with their standard deviations, as we will discuss in the following.

Results

The electrical discharge develops between the HV electrodes and the dielectric surface below, covering the grounded plate. Since both are insulated and the electrodes are moving, the discharge consists in a large number of individual events, when and where breakdown conditions are achieved, with the formation of an ionizing wave propagating in the gap between the electrodes. The electrical discharge then proceeds with the formation of a plasma state and its subsequent quenching as the charged particles reach the dielectric surfaces. Since the driving voltage reverses its sign, also the discharge current inverts itself, continuously sweeping the charges accumulated on the insulating areas. The typical sizes and durations of these micro-discharge events are hundreds of micrometers and tens

of nanoseconds (Siliprandi et al., 2008; Biganzoli et al., 2012). Because of their large number, repetition rate, and slow motion along the plane, each region of the sample is uniformly exposed to the plasma state and interacts with the particles, charged and neutral, composing it. As we discuss in the following, the interaction between the surface of the exposed material and the electrical discharge includes processes like the bombardment by energetic charged particles, ions, and electrons, accelerated by the local electric field as well as the grafting and surface reactions with active chemical species, in particular atomic radicals produced by molecule dissociation in the plasma (Rouette, 1995). In the case of an air discharge, the role of oxidizing (reactive oxidizing species ROS) and more generally (reactive oxygen and nitrogen species RONS) was recognized long ago (Barni et al., 2005). More specifically, when a textile fabric is exposed to the plasma, we could expect both a morphological change in the surface at the nanoscales and a modification in the surface chemical group composition. In particular, textile specimens discussed in the following were treated under the following conditions: head velocity $V = 2.1$ m/min and a number of passes $N = 8$ in air. Together with the applied power level (here $W = 270$ W) and the reactor geometry ($L = 0.22$ m), they could be employed to estimate the average energy delivered to each surface unit of the exposed material, the so-called corona dose,

$$D = \frac{W \times N}{V \times L}, \tag{4}$$

which is used either as a parameter ($D = 280$ kJ/m² from Eq. 4) to compare different plasma treatments or to achieve optimal interaction with the plasma but able to be scaled up to a real industrial process. We also ensured that valuable but delicate textiles like cashmere were not damaged by the electrical discharge.

The chemical properties of the plasma-treated samples have been studied using attenuated total reflectance Fourier transform infrared (FTIR-ATR) spectroscopy, complemented with X-ray photoelectron microscopy (XPS) in our previous studies (see (Zanini et al., 2015; 2018a)). It has been found that the presence of surface oxidation of the plasma-treated fabrics results in enhanced surface wettability. However, the morphological characterization was performed on the treated fibers using SEM only at the micrometer scale (Zanini et al., 2015), and no attempt was made at the sub-micrometer regime, as we are discussing here.

As already stated, one of the finishing effects wanted on the cashmere fabric was a substantial degree of hydro-repellence and oleo-repellence. For this purpose, a fluorocarbon component in the resin is suitable. The SN48 one was sprayed on the original fabric and the plasma-treated one. By visual inspection and optical microscopy, the treated tissues are indistinguishable from the original one.

TABLE 1 Water droplet contact angles measured for treated and untreated cashmere fabrics.

Sample	Finishing	Contact angle [°]
Untreated fabric	No finishing	101 ± 1
Untreated fabric	1% SN48 resin sprayed	142 ± 2
Plasma-treated fabric	1% SN48 resin sprayed	139 ± 4

FIGURE 5
An EDX spectrum recorded from the untreated cashmere fabric sample with its majority components.

The resin coating is sufficient to dramatically increase the water contact angle, measured as discussed in the previous section and reported in Table 1. The values between plasma-treated and untreated fabrics are consistent with the measurement errors. The slightly larger value reported on the sprayed untreated fabric could be related to the differences in their roughness, which we will discuss in the following. However, the true difference made by the plasma action on the textile surface can be seen when polar and apolar kit-tests are performed. As discussed previously, a gradual change in the liquid surface tension could grade precisely the hydro-repellence and oleo-repellence. The results are reported in Table 2 A. The better coating of resin on the fabric surface, probably connected with its texturing induced by the plasma exposure, possibly explains the better outcome. This will be discussed in the following. Another important achievement was obtained when measuring the anti-pilling performances of the treated textiles. As shown in Table 2 B, plasma processing could also help to increase the anti-pilling grade after resin spraying.

An almost point-like measurement of the composition of the coated surface could be performed by EDX analysis (see Figure 5). Small spots were selected from the highest magnification SEM images. To test uniformity in each sample, two different fibers were selected and two spots were chosen, one in the center and the other on the edge of the cuticle. When some bridges of materials joining two adjacent fibers are observed within the images, a spot roughly centered on that feature was selected too. The resin coating could be safely inferred by the presence of foreign atoms, silicon, or fluorine
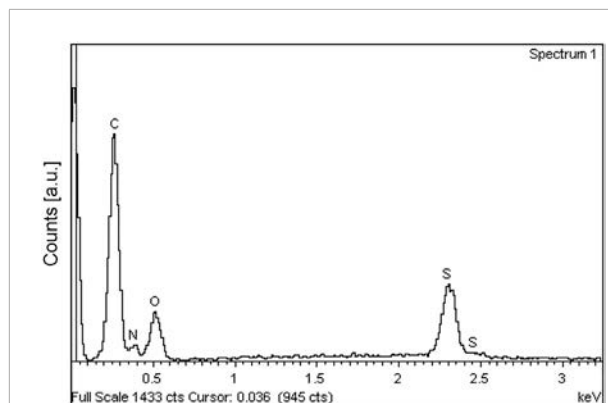
depending on the resin used. The largest concentrations of these elements are reported from the spots centered on the inter-fiber bridges. A few results are collected in Table 3. From them, we can distinguish the effect of the plasma treatment. Although no large excess in resin concentrations is reported on fibers from plasma-treated samples with respect to those from untreated ones, the overall dispersion is much smaller, in particular when comparing the edges of the cuticles. The most convincing explanation lies in a more uniform adhesion and diffusion of the sprayed resins due to the better wettability of the plasma-treated samples (Zanini et al., 2016a). The better uniformity could also explain the increased level of hydro- and oleo-repellency reported previously, in the absence of a larger quantity of resin in the coatings.

So, we are naturally led to investigate how the plasma treatment could modify the adhesion and the uniformity of a finishing process, such as resin spraying. For this purpose, we performed a detailed analysis of the SEM images collected from the fabric samples, briefly introduced in the previous section. For illustration, we show in Figure 6 the images at

TABLE 2 (A) Polar and apolar kit-tests for treated and untreated cashmere fabrics. (B) Anti-pilling grade measured for treated and untreated fabrics.

(A) Sample	Finishing	Polar kit-test	Apolar kit-test
Untreated fabric	No finishing	1.5 ± 0.5	0.0 ± 0.5
Untreated fabric	1% SN48 resin sprayed	5.5 ± 0.5	4.0 ± 0.5
Plasma-treated fabric	1% SN48 resin sprayed	6.0 ± 0.5	6.0 ± 0.5

(B) Sample	Finishing	Pilling test	
Untreated fabric	No finishing	1.0 ± 0.5	
Untreated fabric	1% SN48 resin sprayed	3.0 ± 0.5	
Plasma-treated fabric	1% SN48 resin sprayed	4.0 ± 0.5	
Untreated fabric	1% CNS resin sprayed	3.5 ± 0.5	
Plasma-treated fabric	1% CSN resin sprayed	3.5 ± 0.5	
Untreated fabric	2% CSN resin sprayed	4.0 ± 0.5	
Plasma-treated fabric	2% CSN resin sprayed	4.5 ± 0.5	

TABLE 3 EDX fiber composition (in %) measured on resin-sprayed samples of untreated vs. plasma-treated fabrics at the cuticle edges. The original cashmere composition is reported too.

| Sample	C [%]	O	N	S	Si	F
Untreated fabric	74.4 ± 0.1	14.2 ± 0.1	9.0 ± 0.1	2.6 ± 0.1	0	0
1% SN48 resin sprayed on an untreated fabric	51.6 ± 2.6	16.9 ± 4.4	23.0 ± 0.6	3.2 ± 0.2	0.20 ± 0.02	4.5 ± 2.3
1% SN48 resin sprayed on a plasma-treated fabric	54.4 ± 1.2	22.5 ± 1.4	13.5 ± 2.5	4.5 ± 1.3	0.08 ± 0.04	3.0 ± 0.9
2% CNS resin sprayed on an untreated fabric	57.4 ± 5.8	22.9 ± 1.2	14.9 ± 4.8	3.6 ± 0.8	0.08 ± 0.04	0
2% CNS resin sprayed on a plasma-treated fabric	56.4 ± 1.5	23.5 ± 0.7	15.0 ± 2.1	4.0 ± 0.1	0.09 ± 0.03	0
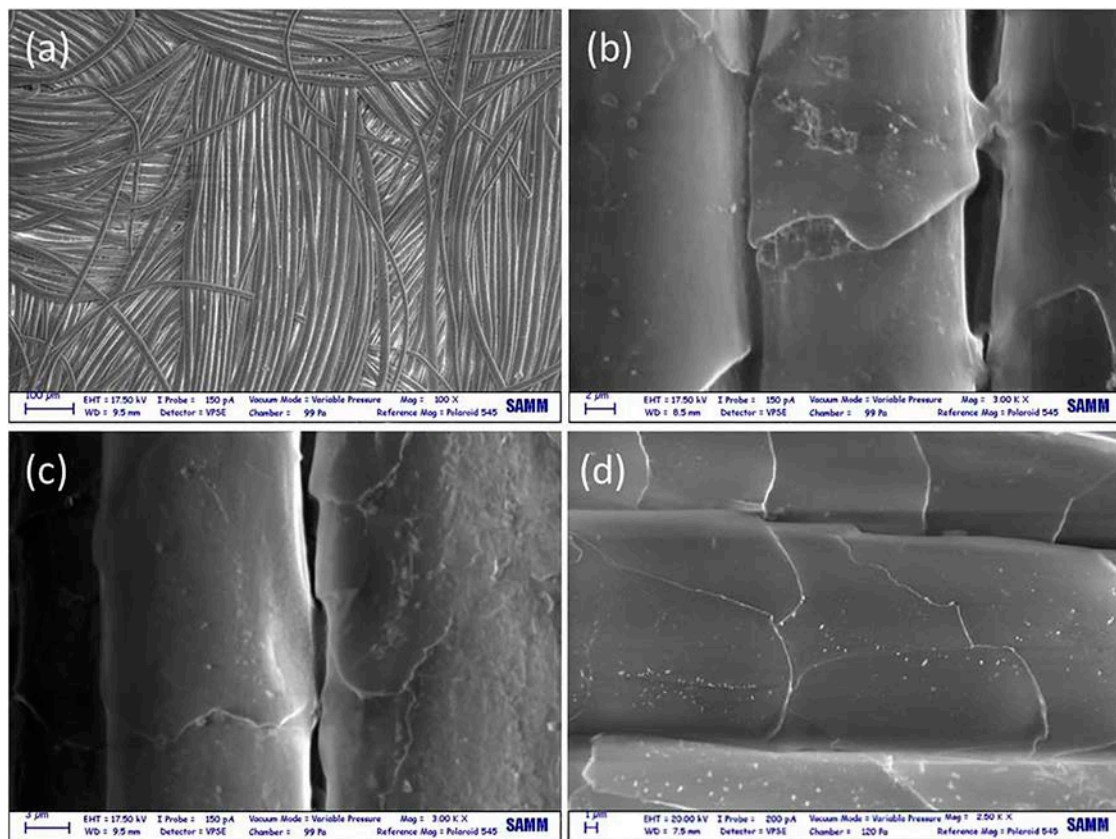
FIGURE 6
SEM image of **(A)** the plasma-treated and subsequently sprayed fabric at low magnification. SEM images at the highest magnification of **(B)** sprayed samples; **(C)** plasma-treated and subsequently sprayed samples; **(D)** plasma-treated-only samples.

the highest magnification of the sprayed, plasma-treated, and plasma-treated and subsequently sprayed samples, together with a low-magnification picture displaying the thread structure of the fabric.

Figure 7 shows the 2D FFT matrices (**Eq. 1**) for an untreated sample, and **Figure 8** shows plasma-treated and resin-sprayed fabrics. It is quite clear that the dominant spatial scales, which

reflect the general morphology of the textile, lay between 100 μm and 1 mm. It is easy to recognize the mostly horizontal and vertical bands (see the arrows in the figure), which are determined by the weaving and warping structure of the textile. Some bent structures can also be grasped, due to the swelling of wool fabrics. This is shown in **Figure 7**, for the untreated fabric. These structures appear to be conserved also after finishing, be it
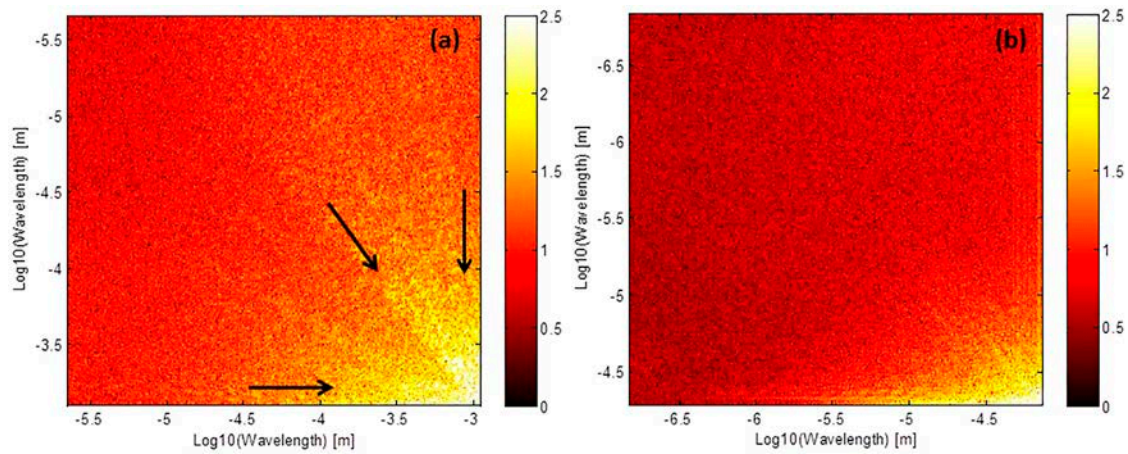
FIGURE 7
FFT bidimensional spectra, $Log_{10}\lambda_y$ vs. $Log_{10}\lambda_x$ (with λ in [m]), measured for the untreated fabric from images at different magnifications: **(A)** ×100 and **(B)** ×1,500. The arrows indicate directions of higher intensity.
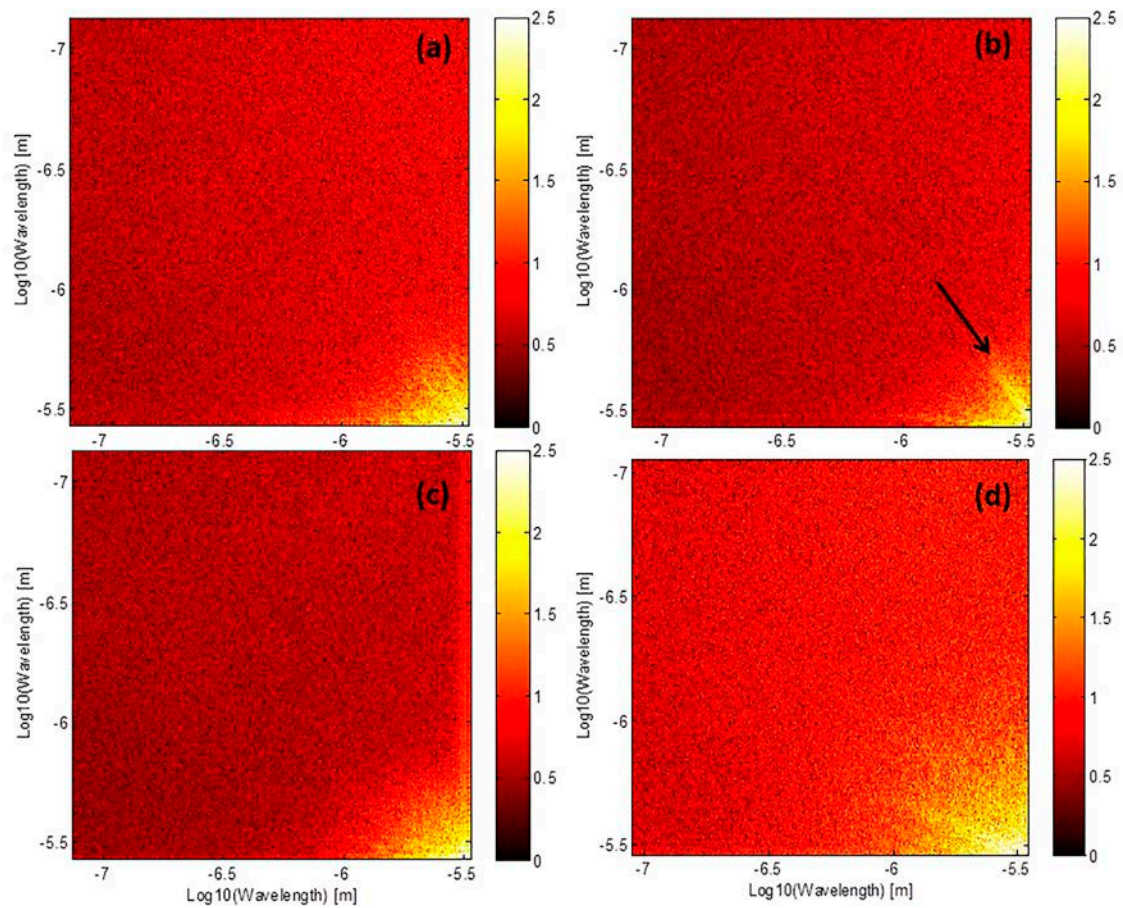

FIGURE 8
FFT bidimensional spectra, $Log_{10}\lambda_y$ vs. $Log_{10}\lambda_x$ (with λ in [m]), measured for **(A)** untreated, **(B)** sprayed, **(C)** plasma-treated and subsequently sprayed, and **(D)** plasma-treated-only samples. In all cases, at sub-micrometer scales, $\lambda < 3\mu$m. The arrow indicates a direction of higher intensity.
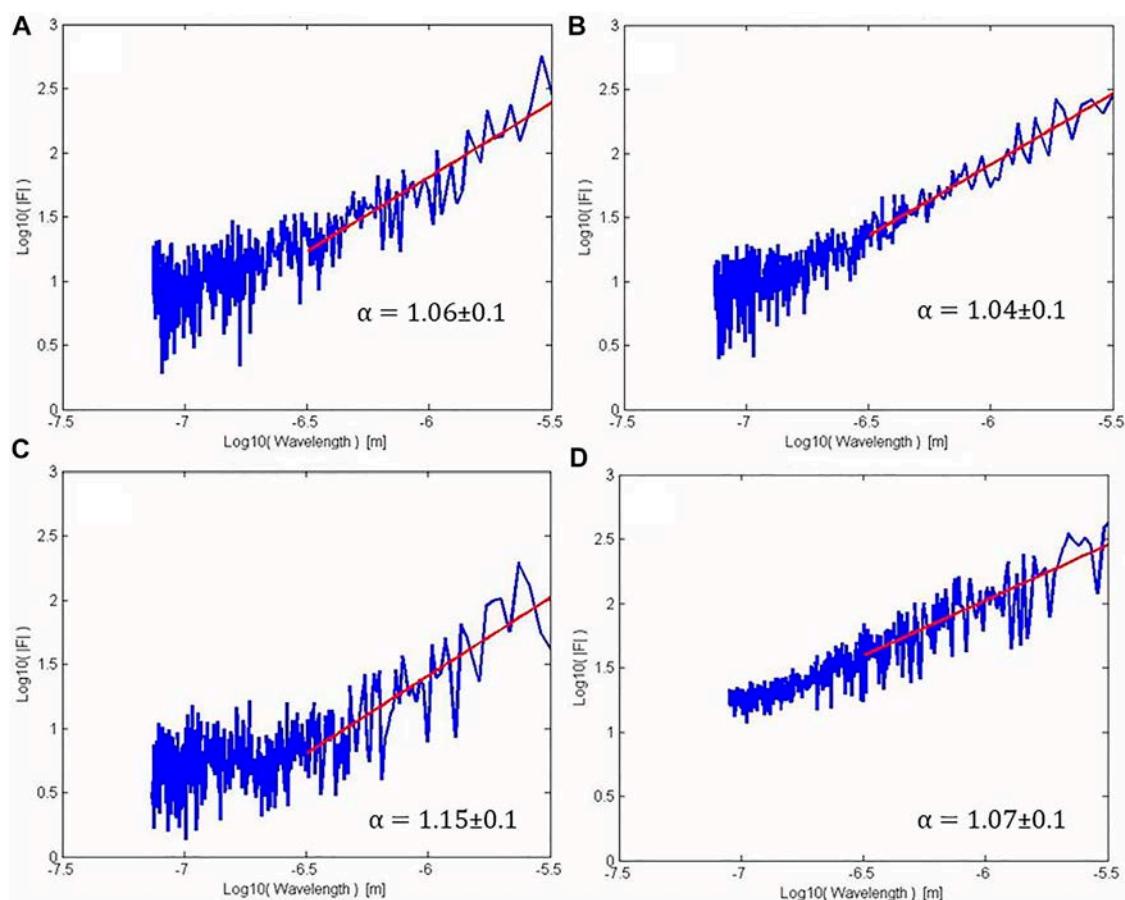
FIGURE 9
FFT spectra, $\log_{10}|F|$ vs. $\log_{10}\lambda$ [m], of different fabrics measured along longitudinal lines for **(A)** untreated, **(B)** sprayed, **(C)** plasma-treated and sprayed, and **(D)** plasma-treated-only samples. The power law fits to the longer scale regions are also shown, and the corresponding values of α are reported in parenthesis.

spraying, plasma exposure, or both. Indeed, we cannot observe any significant difference in FFT, as well as in the SEM images themselves or by visual inspection with optical microscopy of the samples at scales above the fiber size. Because of this general feature dominating the spectra, it is difficult to assess whether there is some structure and/or modification at spatial scales below a few μm. This could be observed in **Figure 8**, with 2D FFT corresponding to the maximum magnification. A single observation is worthy to be pointed out. At a scale around 1 μm, the sample sprayed with resin without any plasma pretreatment shows an oblique band (see arrow in **Figure 8b**), a structure that is not present in the untreated sample as well as in the plasma-treated (resinated or not) ones. This difference could be explained as if the plasma treatment does not change the overall morphology of the textile texture (determined by the warping and weaving processes) but can guide and control resin adhesion, convecting it to the fibers, whereas the direct spraying onto the untreated fabric happens in a more uncontrolled fashion,

with resin lumps covering also and partially masking the fabric texture below. In this sense, plasma treatment keeps the textile morphology and conformation (even after spraying), whereas the direct spraying produces a surface not completely conforming to the original ones, which helps explain why generally resin application could alter the fabric characteristics to somewhat evanescent but is really important for evaluating the fabric merit and value such as touch and softness.

More quantitative information could be assessed using one-dimensional FFT, concerning the longitudinal as well as transverse sections of the fibers. The latter shows the spatial scales connected with the size and the spacing between the fibers. The former are mostly controlled by the interspacing between the cuticles and at a smaller scale by the size of the cuticle superpositions. At the sub-micrometer level, however, the morphology of the single cuticle can be evaluated and the modifications induced by the plasma treatment can be pointed out. In particular, effects like fiber breakings, separation or
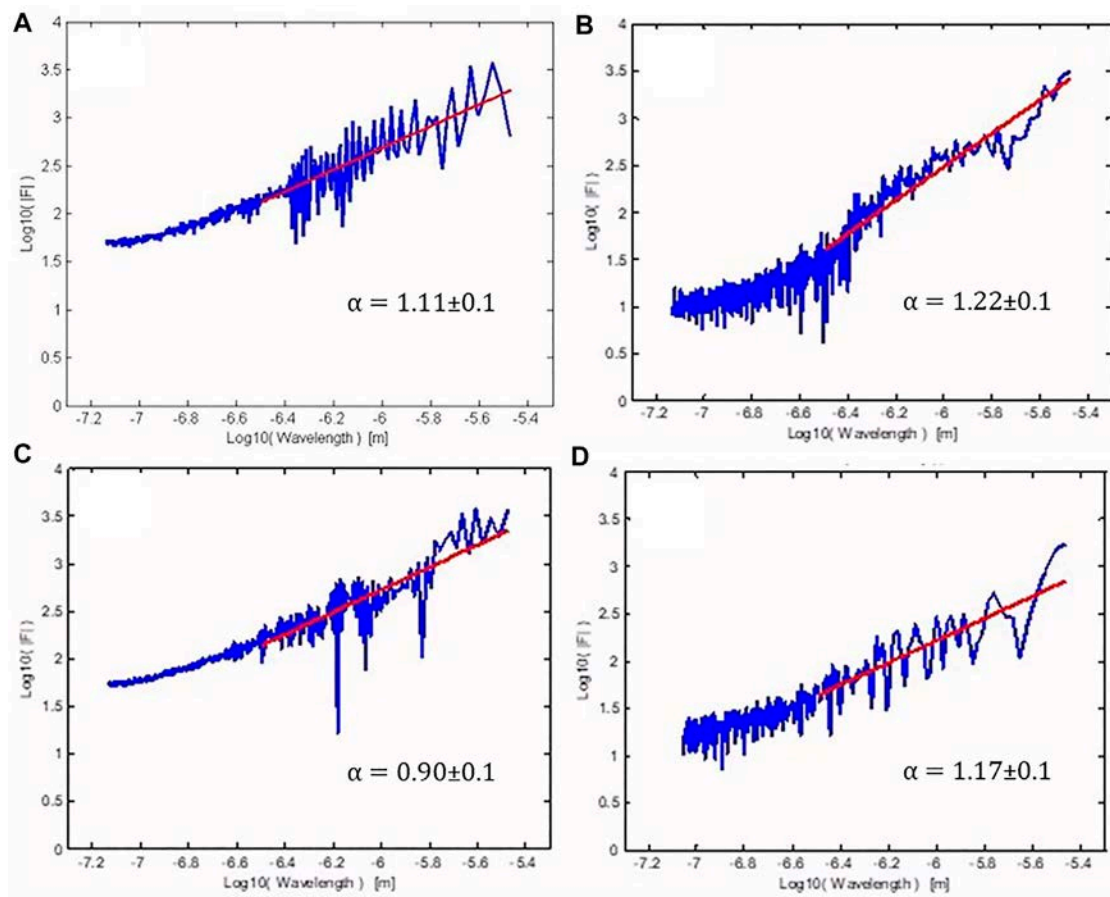
FIGURE 10
FFT spectra, $\text{Log}_{10}|F|$ vs. $\text{Log}_{10}\lambda$ [m], of different fabrics measured along transversal lines for **(A)** untreated, **(B)** sprayed, **(C)** plasma-treated and sprayed, and **(D)** plasma-treated-only samples. The power law fits to the longer scale regions are also shown, and the corresponding values of α are reported in parenthesis.
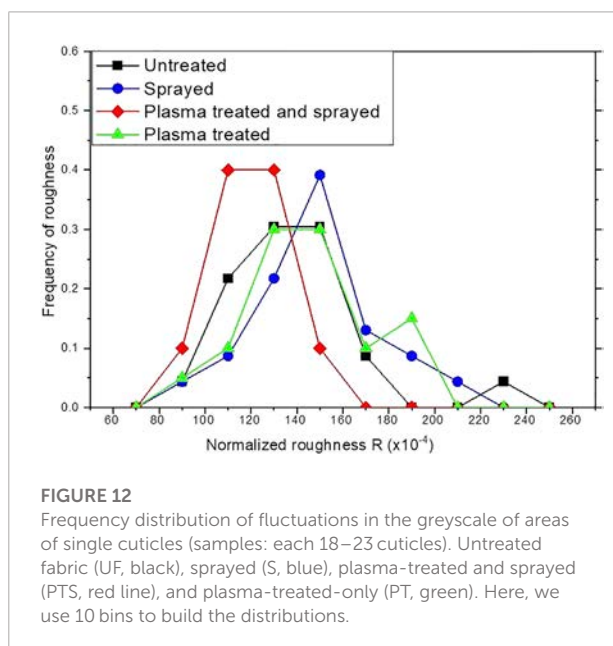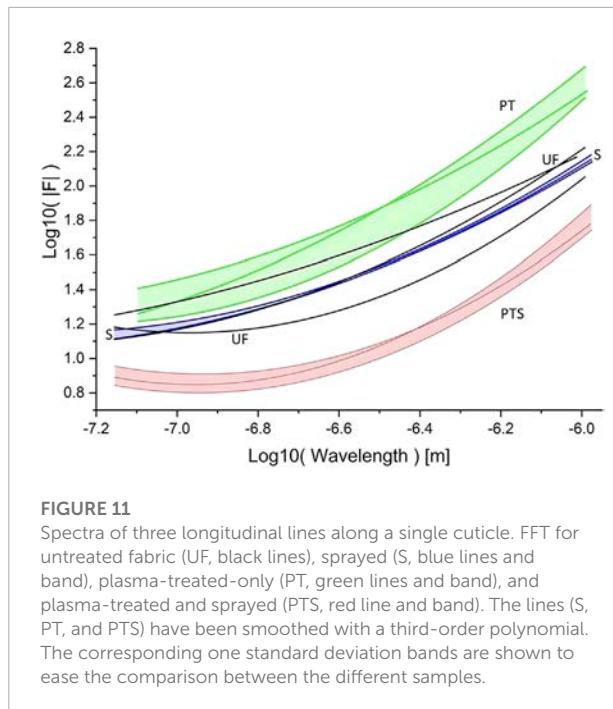
fracturing of the cuticles, formation of holes and craters, and redeposition or formation of dust have to be assessed (Kan and Yuen, 2006; Meade et al., 2008). Also, the possibility of edge abrasion on the cuticles should be evaluated. Our analysis confirms that resin spraying and plasma treatment have only a limited impact on these spatial structures. The cuticle features remain largely unaltered, with no significant instances of both fiber and cuticle fracturing.

As discussed previously, we have proceeded in two complementary ways. After a reorientation of the images, when needed, the longitudinal as well as transverse scales have been measured by integrating the complementary direction or by analyzing a subset of one-dimensional lines vertical (i.e., longitudinal) or horizontal (i.e., transverse). The first important observation was that both methods produced similar results, which supports their strength.

A second observation can be already grasped from **Figure 3**. It is clear that the untreated fibers do not show any particular

structure for scales in the sub-micrometer range. The spectrum is well-reproduced by two power laws, $F \simeq \lambda^\alpha$ (the exponent α corresponds to the straight line on the log–log scale of the picture). This extends to the smallest scales probed by our SEM images, here, about 70 nm. However, it is evident the knee is due to the change in the power law exponent below and above $1\,\mu m$. The trends for large scales show only minor differences between the fibers (for different magnifications, after spraying, with or without plasma treatments). An overall power law with an exponent around one is generally observed for the scales above $1\,\mu m$. For instance, the fitted exponents taken from different parts for two untreated sample images were $\alpha = 0.98 \pm 0.11$ and $\alpha = 1.07 \pm 0.16$, respectively.

We have also investigated the spectra of a large set of selected longitudinal and transverse lines for treated and untreated fabrics, 112 in total. A sample, comparing the spraying and/or the plasma treatment, is shown in **Figures 9**, **10**. For each selected line, the power laws were measured, and the fits are displayed

FIGURE 11
Spectra of three longitudinal lines along a single cuticle. FFT for untreated fabric (UF, black lines), sprayed (S, blue lines and band), plasma-treated-only (PT, green lines and band), and plasma-treated and sprayed (PTS, red line and band). The lines (S, PT, and PTS) have been smoothed with a third-order polynomial. The corresponding one standard deviation bands are shown to ease the comparison between the different samples.

FIGURE 12
Frequency distribution of fluctuations in the greyscale of areas of single cuticles (samples: each 18−23 cuticles). Untreated fabric (UF, black), sprayed (S, blue), plasma-treated and sprayed (PTS, red line), and plasma-treated-only (PT, green). Here, we use 10 bins to build the distributions.

in the figures. All values of α and their spread are consistent within the precision obtained from the single fits. Together with the direct visual inspection of samples and their SEM images, we may conclude that the effect of plasma treatment, resin spraying, and both on large-scale structure is minimal. This confirms that the structure of the cuticle was not altered, in agreement with the overall assessment of SEM imaging, where significant instances of fiber breaking or cuticle fracturing were never spotted.

The main differences thus occur only at the sub-micrometer scales. To ease comparison, a third-degree polynomial smoothing was applied to the spectra for lines in the longitudinal as well as transverse directions. An example is shown in **Figure 11**. As already stated the lines used to extract the spectra are restricted to a single cuticle surface. We could observe a general decrease of the signal with a deviation from the power law at the smaller scales, with a hint of saturation for scales below 300 nm.

The spectrum of the sprayed fabric is practically identical. Also, the spectrum of the plasma-treated sample is similar, but the intensities are slightly larger, indicating a partial roughening induced by the plasma etching. The real novelty is revealed by the spectrum of the plasma-treated fabric and subsequently resin sprayed. In such case, the spectrum is even weaker and its flattening is also more pronounced. This could be explained by a uniform cover of the resin onto the cuticle, characterized by a less structured coating. This does not happen if the surface is not prepared by the plasma treatment. In such case, the resin, which appears to be present on the sample in comparable concentrations, probably glues in the spaces between the fibers or at the cuticle edges. This means that the resin only partially covers the material, which helps to explain why the performances are inferior with respect to the plasma-treated and resinated samples.

The last result was obtained by looking directly at the fluctuations in the greyscale amplitudes measured along a subset of lines, described by the roughness, R (in units of 10^{-4}, see **Eq. 3**), as discussed in the previous section. The roughness frequency distributions for the different samples are shown in **Figure 12**. We observe that resin spraying produces a slight increase in the fluctuation level with respect to the untreated fabric, whereas the same spraying onto the plasma-treated fibers results in a marked decrease of the roughness. This observation agrees with the previous findings that plasma treatment promotes resin adhesion with a larger uniformity and complete covering of the fibers, not achieved by the spraying process alone. We observe also that the plasma treatment in itself does not modify sensibly the fluctuation level, which stays comparable to the one of the untreated sample.

Discussion

The present study performed on pure cashmere textiles demonstrates that resin is able to film the plasma-treated fiber more easily, precisely because of its different surface morphology. There are therefore two important aspects for resin to effectively cover the surface: the resin filming effect which is very important in the coating process and must occur quickly before drying and the physical and chemical bonding effect of resin to the surface. If resin is in the form of a drop on the surface, the coating will not be effective, and the macroscopic property will not be

very efficient. Furthermore, it will be necessary to cover the fiber with a lot of resin, and as a result the coating gets thicker. Thus, the plasma's ability of sizing the fiber has a strong impact on industrial sustainability because it permits saving chemicals and, more importantly, it does not modify the noble character of the fiber.

From the chemical point of view, the plasma treatment in the air promotes a partial oxidation of the fiber surface as already studied in various previous articles. However, the interaction of the molecules and chemical groups with the fiber surface is not the only relevant factor to consider. The explanation lies precisely in the fact that the increase in surface tension (i.e., low contact angle) is not only due to a modified chemical property, but also due to the morphological modification of the surface. The aim of our study is to understand the mechanisms of improvement after plasma treatment of the fiber. We find that in addition to partial oxidation widely studied in the literature, the plasma modifies the surface on the nanoscale, as evidenced by the spectral forms.

Another important consequence is the quality of the coating: using a fluorinated resin, it was possible to obtain unique hydro/oleo-repellent properties and pilling, without altering the hand assessment quality of the textile, which is a compelling feature of such a noble fabric.

Conclusion

Pure cashmere fabrics have been exposed to an electric discharge. Atmospheric plasma treatments were effectual in the modification of the textile surface at the nanometer scale. As we have discussed, the differences in the nano-texturing induced by the surface etching promoted by the interaction with the plasma are relevant in the subsequent finishing processes when resins are sprayed onto the textiles. More stable, uniform, and effectual coating by the resins was observed, leading to improved properties of the finishing, both regarding hydro- and oleo-repellency, which are highly prized for these rather valued textiles. The appearance of a nano-structuring of the surface of the fiber improves the interaction of the fluid (resin) with the fiber. This effect favors the flow of the liquid before drying with the result of a better covering of the fibers (filming).

More generally, these results underline the perspective that dry, efficient, and eco-friendly plasma technology opens a wide range of new possibilities also for the quite mature textile industrial sector. It could also be used to boost the efficiency of finishing processes normally discarded, such as spraying versus immersion, for resin adhesion, as in our case. Indeed, the oleo-repellency grade we obtained is better than the best reported after resin impregnation as discussed in the

literature (Zanini et al., 2016a). As we tried to point out, this happens because of the plasma action at the atomic level, which produces features at the nanoscales, while generally not erasing the structure, morphology, and composition of the treated material, even in the case of complex, biological fibers such as cashmere.

Data availability statement

The raw data supporting the conclusion of this article will be made available by the authors, without undue reservation.

Author contributions

CR and AC contributed to the conception and design of the study. RB and GL organized the database. RB and HER performed the statistical analysis. RB and CR wrote the first draft of the manuscript. All authors wrote sections of the manuscript. All authors contributed to manuscript revision, read, and approved the submitted version.

Funding

Acknowledgments

Conflict of interest

The authors declare that the research was conducted in the absence of any commercial or financial relationships that could be construed as a potential conflict of interest.

Publisher's note

References

Abramova, A. V., Abramov, V. O., Bayazitov, V. M., Voitov, Y., Straumal, E. A., Lermontov, S. A., et al. (2020). A sol–gel method for applying nanosized antibacterial particles to the surface of textile materials in an ultrasonic field. *Ultrason. Sonochemistry* 60, 104788. doi:10.1016/j.ultsonch.2019.104788

ASTM (2017). Standard test method for pilling resistance and other related surface changes of textile fabrics: Random tumble pilling tester. *ASTM* 07, D76–D4391. doi:10.1520/D3512-02

Barni, R., Esena, P., and Riccardi, C. (2005). Chemical kinetics simulation for atmospheric pressure air plasmas in a streamer regime. *J. Appl. Phys.* 97, 073301. doi:10.1063/1.1879081

Biganzoli, I., Barn, R., and Riccardi, C. (2012). Temporal evolution of a surface dielectric barrier discharge for different groups of plasma microdischarges. *J. Phys. D. Appl. Phys.* 46, 025201. doi:10.1088/0022-3727/46/2/025201

Biganzoli, I., Barni, R., Riccardi, C., Gurioli, A., and Pertile, R. (2013b). Optical and electrical characterization of a surface dielectric barrier discharge plasma actuator. *Plasma Sources Sci. Technol.* 22, 025009. doi:10.1088/0963-0252/22/2/025009

Biganzoli, I., Barni, R., and Riccardi, C. (2013a). Note: On the use of Rogowski coils as current probes for atmospheric pressure dielectric barrier discharges. *Rev. Sci. Instrum.* 84, 016101. doi:10.1063/1.4773233

Brigham, E. O. (1988). *The fast Fourier transform and its applications*. New Jersey, United States: Prentice-Hall.

Bulut, M. O., and Sana, N. H. (2018). Modification of woolen fabric with plasma for a sustainable production. *Fibers Polym.* 19, 1887–1897. doi:10.1007/s12221-018-8488-1

Dell'Orto, E. C., Caldirola, S., Sassella, A., Morandi, V., and Riccardi, C. (2017). Growth and properties of nanostructured titanium dioxide deposited by supersonic plasma jet deposition. *Appl. Surf. Sci.* 425, 407–415. doi:10.1016/j.apsusc.2017.07.059

Dell'Orto, E. C., Vaccaro, A., and Riccardi, C. (2014). Morphological and chemical analysis of PP film treated to Dielectric Barrier Discharge. *J. Phys. Conf. Ser.* 550, 012032. doi:10.1088/1742-6596/550/1/012032

Haji, A. (2020a). Application of D-optimal design in the analysismodelinglling of dyeing of plasma-treated wool with three natural dyes. *Color. Technol.* 136, cote.12445–146. doi:10.1111/cote.12445

Haji, A., Ashraf, S., Nasiriboroumand, M., and Lievens, C. (2020). Environmentally friendly surface treatment of wool fiber with plasma and chitosan for improved coloration with cochineal and safflower natural dyes. *Fibers Polym.* 21, 743–750. doi:10.1007/s12221-020-9587-3

Haji, A. (2020b). Natural dyeing of wool with henna and yarrow enhanced by plasma treatment and optimized with response surface methodology. *J. Text. Inst.* 111, 467–475. doi:10.1080/00405000.2019.1642710

Heinzel, T., and Stewart, R. (2021). Introduction: Textile intersections–textile discipline at cross–roads. *J. Text. Des. Res. Pract.* 9, 1–8. doi:10.1080/20511787.2021.1914392

James, E. (2022). *Using FFT to quantify differences in spatial frequency of gray scale images*. Natick, MA, US.: Matlab Newsgroup. Availabe at: http://www.mathworks.it.

Kan, C. W., and Yuen, C. W. M. (2006). Retracted: Dyeing behaviour of low temperature plasma treated wool. *Plasma process. Polym.* 3, 627–635. doi:10.1002/ppap.200600086

Khoso, A. N., Memon, H., Hussain, M., Sanbhal, A. N., and Abro, A. (2016). Production and characterization of wool and hair fibers in highlands of baluchistan, an economic and sustainable approach for Pakistan. *Key Eng. Mat.* 671, 473–482. doi:10.4028/www.scientific.net/kem.671.473

Kogelschatz, U. (2003). Dielectric-barrier discharges: Their history, discharge physics, and industrial applications. *Plasma Chem. plasma Process.* 23, 1–46. doi:10.1023/A:1022470901385

Le, C. V., Ly, N. G., and Stevens, M. G. (1996). Measuring the contact angles of liquid droplets on wool fibers and determining surface energy components. *Text. Res. J.* 66, 389–397. doi:10.1177/004051759606600606

Leeder, J. D. (1984). *Wool: Nature's wonder fibre*. Australia: Australasian Textiles Publishers.

Liu, L., Wang, S., Huang, H., Zhang, Y., and Ma, T. (2020). Surface sites engineering on semiconductors to boost photocatalytic CO_2 reduction. *Nano Energy* 75, 104959. doi:10.1016/j.nanoen.2020.104959

Meade, S. J., Dyer, J. M., Caldwell, J. P., and Bryson, W. G. (2008). Covalent modification of the wool fiber surface: Removal of the outer lipid layer. *Text. Res. J.* 78, 943–957. doi:10.1177/0040517507087859

Memon, H., Wang, H., and Langat, E. K. (2018a). Determination and characterization of the wool fiber yield of kenyan sheep breeds: An economically sustainable practical approach for Kenya. *Fibers* 6, 55. doi:10.3390/fib6030055

Memon, H., Wang, H., Yasin, S., and Halepoto, A. (2018b). Influence of incorporating silver nanoparticles in protease treatment on fiber friction, antistatic, and antibacterial properties of wool fibers. *J. Chem.* 2018, 1–8. doi:10.1155/2018/4845687

Murakami, G. D., Jinnai, H., and Takahara, A. (2014). Wetting transition from the cassie–baxter state to the wenzel state on textured polymer surfaces. *Langmuir* 30, 2061–2067. doi:10.1021/la4049067

Nagayama, G., and Zhang, D. (2020). Intermediate wetting state at nano/microstructured surfaces. *Soft Matter* 16, 3514–3521. doi:10.1039/C9SM02513H

Najar, S. S., Wang, X., and Naebe, M. (2018). The effect of plasma treatment and tightness factor on the low-stress mechanical properties of single Jersey knitted wool fabrics. *Text. Res. J.* 88, 499–509. doi:10.1177/0040517516681962

Noman, M. T., Amor, N., Petru, M., Mahmood, A., and Kejzlar, P. (2021). Photocatalytic behaviour of zinc oxide nanostructures on surface activation of polymeric fibres. *Polymers* 13, 1227. doi:10.3390/polym13081227

Peng, L., Chen, W., Su, B., Yu, A., and Jiang, X. (2019). Cs_xWO_3 nanosheet–coated cotton fabric with multiple functions: UV/NIR shielding and full–spectrum–responsive self–cleaning. *Appl. Surf. Sci.* 475, 325–333. doi:10.1016/j.apsusc.2018.12.279

Peran, J., Ražić, S. E., Sutlović, A., Ivanković, T., and Glogar, M. I. (2020). Oxygen plasma pretreatment improves dyeing and antimicrobial properties of wool fabric dyed with natural extract from pomegranate peel. *Color. Technol.* 136, cote.12464–187. doi:10.1111/cote.12464

Piferi, C., Barni, R., Roman, H. E., and Riccardi, C. (2021). Current filaments in asymmetric surface dielectric barrier discharge. *Appl. Sci.* 11, 2079. doi:10.3390/app11052079

Porto, C. L., Di Mundo, R., Veronico, V., Trizio, I., Barucca, G., and Palumbo, F. (2019). Easy plasma nano–texturing of PTFE surface: From pyramid to unusual spherules–on–pyramid features. *Appl. Surf. Sci.* 483, 60–68. doi:10.1016/j.apsusc.2019.03.220

Radetić, M., and Marković, D. (2019). Nano-finishing of cellulose textile materials with copper and copper oxide nanoparticles. *Cellulose* 26, 8971–8991. doi:10.1007/s10570-019-02714-4

Rouette, H. K. (1995). "Wool," in *Encyclopedia of textile finishing*. Editor H. K. Rouette (Netherland: Elsevier).

Saleem, H., and Zaidi, S. J. (2020). Sustainable use of nanomaterials in textiles and their environmental impact. *Materials* 13, 5134. doi:10.3390/ma13225134

Siliprandi, R., Roman, H. E., Barni, R., and Riccardi, C. (2008). Characterization of the streamer regime in dielectric barrier discharges. *J. Appl. Phys.* 104, 063309. doi:10.1063/1.2978184

Singh, M., Vajpayee, M., and Ledwani, L. (2020). "Eco–friendly surface modification and nanofinishing of textile polymers to enhance functionalisation," in *Nanotechnology for energy and environmental engineering. Green energy and*

technology. Editors L. Ledwani, and J. Sangwai (Cham, Switzerland: Springer), 529–559. doi:10.1007/978-3-030-33774-2_23

Trifiletti, V., Ruffo, R., Turrini, C., Tassetti, D., Brescia, R., Di Fonzo, F., et al. (2013). Dye-sensitized solar cells containing plasma jet deposited hierarchically nanostructured tio$_2$ thin photoanodes. *J. Mat. Chem. A Mat.* 1, 11665–11673. doi:10.1039/C3TA11485F

Venkatraman, P. D., Sayed, U., Parte, S., and Korgaonkar, S. (2021). Development of advanced textile finishes using nano–emulsions from herbal extracts for organic cotton fabrics. *Coatings* 11, 939. doi:10.3390/coatings11080939

Wang, H., Farha, F. I., and Memon, H. (2020). Influence of ultraviolet irradiation and protease on scale structure of alpaca wool fibers. *Autex Res. J.* 20, 476–483. doi:10.2478/aut-2019-0039

Wang, X., Zhuang, L., Jia, Y., Liu, H., Yan, X., Zhang, L., et al. (2018). Plasma–triggered synergy of exfoliation, phase transformation, and surface engineering in cobalt diselenide for enhanced water oxidation. *Angew. Chem. Int. Ed.* 57, 16421–16425. doi:10.1002/anie.201810199

Zanini, S., Citterio, A., Leonardi, G., and Riccardi, C. (2018a). Characterization of atmospheric pressure plasma treated wool/cashmere textiles: Treatment in nitrogen. *Appl. Surf. Sci.* 427, 90–96. doi:10.1016/j.apsusc.2017.07.280

Zanini, S., Freti, S., Citterio, A., and Riccardi, C. (2016a). Characterization of hydro-and oleo–repellent pure cashmere and wool/nylon textiles obtained by atmospheric pressure plasma pre–treatment and coating with a fluorocarbon resin. *Surf. Coatings Technol.* 292, 155–160. doi:10.1016/j.surfcoat.2016.03.020

Zanini, S., Grimoldi, E., Citterio, A., and Riccardi, C. (2015). Characterization of atmospheric pressure plasma treated pure cashmere and wool/cashmere textiles: Treatment in air/water vapor mixture. *Appl. Surf. Sci.* 349, 235–240. doi:10.1016/j.apsusc.2015.05.010

Zanini, S., Zoia, L., Della Pergola, R., and Riccardi, C. (2018b). Pulsed plasma–polymerized 2–isopropenyl–2–oxazoline coatings: Chemical characterization and reactivity studies. *Surf. Coatings Technol.* 334, 173–181. doi:10.1016/j.surfcoat.2017.11.044

Zanini, S., Zoia, L., Dell'Orto, E. C., Natalello, A., Villa, A. M., Della Pergola, R., et al. (2016b). Plasma polymerized 2–ethyl–2–oxazoline: Chemical characterization and study of the reactivity towards different chemical groups. *Mater. Des.* 108, 791–800. doi:10.1016/j.matdes.2016.07.051

Zhao, T., Li, J., Zeng, H., Fu, Y., He, H., Xing, L., et al. (2018). Self–powered wearable sensing-textiles for real-time detecting environmental atmosphere and body motion based on surface–triboelectric coupling effect. *Nanotechnology* 29, 405504. doi:10.1088/1361-6528/aad3fc